Waveguide fabrication in lfithium-niobo-phosphate glasses by high repetition rate femtosecond laser: route to non-equilibrium material's states

Mykhaylo Dubov,[1,*] **Vladimir Mezentsev,**[1] **Alina A. Manshina,**[2]
Ivan A. Sokolov,[2] **Alexey V. Povolotskiy** [2] **and Yuri V. Petrov**[3,4]

[1]*Aston Institute of Photonic Technologies, School of Engineering and Applied Science,*
Aston University, Birmingham B4 7ET, UK
[2]*Chemical department, St.Petersburg State University, St.Petersburg, Russia*
[3]*Interdisciplinary Resource Center for Nano-Technology, St.Petersburg State University, &*
[4]*St.Petersburg State Polytechnical University, St.Petersburg, Russia*

[*]*m.dubov@aston.ac.uk*

Abstract: We study waveguide fabrication in lithium-niobo-phosphate glass, aiming at a practical method of single-stage fabrication of nonlinear integrated-optics devices. We observed chemical transformations or material redistribution during the course of high repetition rate femtosecond laser inscription. We believe that the laser-induced ultrafast heating and cooling followed by elements diffusion on a microscopic scale opens the way toward the engineering non-equilibrium sates of matter and thus can further enhance Refractive Index (RI) contrasts by virtue of changing glass composition in and around the fs tracks.

OCIS codes: (130.2755) Glass waveguides; (160.2750) Glass and other amorphous materials.

References and links

1. H. Misawa and S. Juodkazis, eds., *3D Laser Microfabrication. Principles and Applications* (Wiley-VCH, Weinheim, 2006).
2. R. Osellame, G. Cerullo, and R. Ramponi, *Femtosecond Laser Micromachining: Photonic and Microfluidic Devices in Transparent Materials*, SpringerLink : Bücher (Springer Berlin Heidelberg, 2012).
3. V. Mezentsev, J. Petrovic, M. Dubov, I. Bennion, J. Dreher, H. Schmitz, and R. Grauer, "Femtosecond laser microfabrication of subwavelength structures in photonics," Proc. SPIE **6459**, 64590B (2007).
4. A. V. Turchin, M. Dubov, and J. A. R. Williams, "In situ measurement and reconstruction in three dimensions of femtosecond inscription-induced complex permittivity modification in glass," Opt. Lett. **35**, 2952–2954 (2010).
5. A. V. Turchin, M. Dubov, and J. Williams, "3D reconstruction of the complex dielectric function of glass during femtosecond laser micro-fabrication," Optical and Quantum Electronics **42**, 873–886 (2011).
6. V. Mizeikis, S. Kimura, N. V. Surovtsev, V. Jarutis, A. Saito, H. Misawa, and S. Juodkazis, "Formation of amorphous sapphire by a femtosecond laser pulse induced micro-explosion," Applied Surface Science **255**, 9745–9749 (2009).
7. L. B. Glebov, V. I. Smirnov, C. M. Stickley, and I. V. Ciapurin, "New approach to robust optics for HEL systems," Proc. SPIE **4724**, 101–109 (2002).
8. S. M. Eaton, H. Zhang, M. L. Ng, J. Li, W.-J. Chen, S. Ho, and P. R. Herman, "Transition from thermal diffusion to heat accumulation in high repetition rate femtosecond laser writing of buried optical waveguides," Opt. Express **16**, 9443–9458 (2008).
9. S. M. Eaton, M. L. Ng, J. Bonse, A. Mermillod-Blondin, H. Zhang, A. Rosenfeld, and P. R. Herman, "Low-loss waveguides fabricated in BK7 glass by high repetition rate femtosecond fiber laser," Appl. Opt. **47**, 2098–2102 (2008).

10. T. Allsop, M. Dubov, V. Mezentsev, and I. Bennion, "Inscription and characterization of waveguides written into borosilicate glass by a high-repetition-rate femtosecond laser at 800 nm," Appl. Opt. **49**, 1938–1950 (2010).
11. M. Sakakura, M. Terazima, Y. Shimotsuma, K. Miura, and K. Hirao, "Heating and rapid cooling of bulk glass after photoexcitation by a focused femtosecond laser pulse," Opt. Express **15**, 16800–16807 (2007).
12. A. Pasquarello and R. Car, "Identification of Raman defect lines as signatures of ring structures in vitreous silica," Physical Review Letters **80**, 5145–5147 (1998).
13. D. J. Little, M. Ams, P. Dekker, G. D. Marshall, and M. J. Withford, "Mechanism of femtosecond-laser induced refractive index change in phosphate glass under a low repetition-rate regime," Journal of Applied Physics **108**, 033110 (2010).
14. S. Gross, D.G. Lancaster, H. Ebendorff-Heidepriem, T.M. Monro, A. Fuerbach, and M.J. Withford, "Femtosecond laser induced structural changes in fluorozirconate glass," Opt. Mater. Express **3**, 574–583 (2013).
15. I. Sokolov, Y. Tarlakov, N. Ustinov, N. Valova, and A. Pronkin, "Influence of the nature of an alkali cation on the electrical conductivity of vitreous $MePO_3$ (Me = Li, Na, or K)," Glass Physics and Chemistry **29**, 305–309 (2003).
16. A. K. Varshneya, *Fundamentals of Inorganic Glasses* (Academic Press Inc., 1994).
17. C. Ziling, L. Pokrovskii, N. Terpugov, I. Savatinova, M. Kuneva, S. Tonchev, M. N. Armenise, and V. M. N. Passaro, "Optical and structural properties of annealed $PE:LiNbO_3$ waveguides formed with pyrophosphoric and benzoic acids," Journal of Applied Physics **73**, 3125–3132 (1993).
18. A. Fernandez, T. Fuji, A. Poppe, A. Frbach, F. Krausz, and A. Apolonski, "Chirped-pulse oscillators: a route to high-power femtosecond pulseswithout external amplification," Opt. Lett. **29** 1366–1368 (2004).
19. R. Graf, A. Fernandez, M. Dubov, H. Brueckner, B. Chichkov, and A. Apolonski, "Pearl-chain waveguides written at megahertz repetition rate," Applied Physics B: Lasers and Optics **87**, 21–27 (2007).
20. W. Yang, P. G. Kazansky, Y. Shimotsuma, M. Sakakura, K. Miura, and K. Hirao, "Ultrashort-pulse laser calligraphy," Applied Physics Letters **93**, 171109 (2008).
21. J. Goldstein, *Scanning Electron Microscopy and X-Ray Microanalysis* (Springer London, Limited, 2003).
22. D. Drouin, A. R. Couture, D. Joly, X. Tastet, V. Aimez, and R. Gauvin, "CASINO v 2.42a. A fast and easy-to-use modeling tool for scanning electron microscopy and microanalysis users," Scanning **29**, 92–101 (2007).
23. T. Uchino and T. Yoko, "Structure and vibrational properties of alkali phosphate glasses from ab initio molecular orbital calculations," Journal of Non-Crystalline Solids **263–264**, 180–188 (2000).
24. E. Kartini, T. Y. S. P. Putra, I. Kuntoro, T. Sakuma, K. Basar, O. Kamishima, and J. Kawamura, "Recent studies on lithium solid electrolytes $(LiI)_x(LiPO_3)_{1-x}$ for secondary battery," Journal of the Physical Society of Japan **79SA**, 54–58 (2010).
25. J. Li, Z. Sun, X. Zhu, H. Zeng, Z. Xu, Z. Wang, J. Lin, W. Huang, R. S. Armstrong, and P. A. Lay, "Optical bistability for $ZnO-Nb_2O_5-TeO_2$ glasses," Optical Materials **25**, 401–405 (2004).
26. N. K. Mohan, M. R. Reddy, C. Jayasankar, and N. Veeraiah, "Spectroscopic and dielectric studies on MnO doped $PbO-Nb_2O_5-P_2O_5$ glass system," Journal of Alloys and Compounds **458**, 66–76 (2008).
27. I. Mazali, L. Barbosa, and O. Alves, "Preparation and characterization of new niobophosphate glasses in the $Li_2O-Nb_2O_5-CaO-P_2O_5$ system," Journal of Materials Science **39**, 1987–1995 (2004).
28. R. R. Rakhimov, V. J. Turney, D. E. Jones, S. N. Dobryakov, Y. A. Borisov, A. I. Prokofev, and A. I. Aleksandrov, "Electron paramagnetic resonance and quantum-mechanical analysis of binuclear niobium clusters in lithiumniobium phosphate glasses," The Journal of Chemical Physics **118**, 6017–6021 (2003).
29. F. Cotton and G. Wilkinson, *Advanced Inorganic Chemistry* (Wiley, New York, 1999).
30. S. C. Abrahams and P. Marsh, "Defect structure dependence on composition in lithium niobate," Acta Crystallographica Section B **42**, 61–68 (1986).

1. Introduction

Micro-fabrication of photonics devices by means of intense femtosecond (fs) laser pulses has emerged as a novel technology during the last decade [1, 2]. It has quickly become one of the most powerful and diverse methods for micro- and even nano-fabrication. A range of photonic structures and devices has been demonstrated recently based on permanent modification of refractive index after fs inscription (see e.g. [2, 3] and references therein). This enabling technology significantly expands the technological boundaries for direct fabrication of photonics structures in a wide variety of materials, as it allows modification of virtually any non-photosensitive transparent material, thus opening the door to numerous practical applications [2]. Its uniqueness is based on three physical facts: i) nonlinear absorption, which triggers the energy deposition only at or around a focal point inside a sample; ii) the density of energy deposited in such processes can exceed that typically achieved by the majority of other methods; iii) the rates of energy deposition and following cooling are also extremely high, potentially leading to

non-equilibrium phase transitions and states of materials, which otherwise cannot be obtained in a laboratory.

For example, ultrafast cooling of a borosilicate glass [4, 5] after an exposure to either a multiple pulses or after just a single pulse in sapphire [6], revealed a creation of a nano-crystalline precursors of phases, which can only be obtained in bulk materials under very high pressures and temperatures. It is this third point which was a motivation for this work, as High Repetition Rate (HRR), direct fs inscription, imposing unique conditions, could lead to a creation of non-equilibrium phases of material. Given the speed of such transitions, they may result in mixture of precursor phases, which may be of interest for nonlinear optics applications (as the nonlinear optics in general and nonlinear materials in particular become more and more demanded for ultrafast signal manipulation in modern telecom and quantum optics devices). For example, some glasses allow precipitation of nano-particles or nano-crystals formation in two-stage process, like in photo-thermo-refractive glasses [7] the NaF nano-crystals grow in silica matrix. One can expect that intensive heating and high pressures, produced by direct fs inscription at high-repetition rate [8–10], can trigger similar transformations but in a single-stage process, which may be an advantage. Laser-induced crystallization under HRR fs irradiation has not been widely explored yet, but it could result in a stronger nonlinear response of the media. If a waveguide can be created during such a treatment, it could provide easy access for and light guiding through those modified regions at the same time.

In this paper we discuss an approach for achievement of high refractive index contrast based on laser induced alternation of local chemical composition of the optical material caused by chemical elements diffusion. Change of chemical composition due to the diffusion [11] can result in much stronger optical parameters variation in comparison with the case of structural reorganization [12, 13], which is more characteristic to low-repetition rate fs microfabrication. The structural rearrangements as a result of HRR fs laser inscription have also been observed in various glasses, for example in ZBLAN glass [14], where it was found that the rarefaction of the glass network decreased the material density and WGs demonstrate negative refractive index contrast. Local ions diffusion in bulk glass can be induced by laser ultrafast heating and highly localised melting of the material, at that the diffusion length and rate are determined by temperature gradient, time of treatment (e.g. cooling rate) and nature of chemical species. As these parameters can be controlled by optimizing laser power, sample translation speed and glass chemical composition, laser induced elements/ions diffusion can be considered as efficient way of high contrast optical phase elements creation.

Lithium Niobo Phosphate (LNP) glasses appear as a promising class of potentially highly-nonlinear niobophosphate glass, with a rich variety of chemical-physical properties including a possibility of creation of nonlinear nano-crystals. Such glasses may have compositions e.g. 0.25–$0.5\,Li_2O$–0.35–$0.1\,Nb_2O_5$–$0.4\,P_2O_5$, with 25/50 35/10 and 40 weight percent (wt %) respectively. A number of such LNP glasses have been synthesized with variable compositions of Li (as well as K and Na), but for this brief communication no comparison between those families will be given. Among the ready-to-diffuse chemical elements alkali ions stand out. Their mobility rate is increase in the progression K–Na–Li. It explains the reason for using Li ions in first experiments on laser-induced diffusion [15]. As a glassy host phosphate matrix was chosen since it is characterized by high diffusion parameters of alkali ions and has satisfying chemical stability [16]. The choice of phosphate matrix P_2O_5 as a glassy host was made due to its chemical stability and flexibility in terms of accommodation of much higher concentrations of different dopants without their clustering. The latter is often a problem in silicate glasses. The phase diagrams of such glasses are mostly unknown, especially at high temperatures and pressures. However, earlier studies revealed a variety of phase precursors created in similar matrices at different conditions, for example lithium meta-niobate (LiNbO) [17].

For increase of glass chemical stability and refractive index value niobium oxide was added [17]. Moreover alkali ions (Li) and Nb_2O_5 in glass network tend to form structural fragments of lithium metaniobate ($LiNbO_3$) what determines the main physicochemical properties of glasses, including high mobility of alkali ions. So for the experiments on fs laser writing of high contrast optical phase elements glass sample with composition $0.5\,Li_2O$–$0.4\,P_2O_5$–$0.1\,Nb_2O_5$ was synthesized.

In this paper we first study waveguide fabrication in LNP glass, aiming at a practical method of single-stage fabrication of integrated, nonlinear optics devices. We also observe an evidence of chemical transformations or material redistribution during the course of laser treatment. We believe that the laser-induced heating followed by elements diffusion can be efficient way to increase Refractive Index (RI) contrasts by virtue of changing glass composition around the fs tracks.

2. Experimental procedures

2.1. Glass synthesis

Nb_2O_5, Li_2CO_3, $(NH_4)_2HPO_4$ elements of analytical grade purity were used as raw materials for preparation of the glass samples $0.5Li_2O$–$0.1Nb_2O_5$–$0.4P_2O_5$. At the first stage $(NH_4)_2HPO_4$ compound was kept at $500°C$ for 2-3 hours for NH3 and sorbed H2O removal in order to avoid the possible Nb^{5+} to Nb^{4+}/Nb^{3+} reduction. Glass synthesis was carried out by using a conventional melt-quenching method in alundum crucible at temperature $1100\ °C$ during 1.5 - 2 hours. The melt was poured onto heated up to $250\ °C$ iron plate. Then the glass on the plate was kept in an electric furnace at $270\ °C$ for 4 hours and cooled down for 10 hours. The glass obtained was polished into samples with thickness 2 mm.

2.2. Laser system and femtosecond inscription

Femtosecond Ti:Sapphire laser system used in this work is a commercial chirped-pulse oscillator (Femtolaser). It operates at about 800 nm wavelength, and is capable of delivering of output power of 1.2 W, or 11 MHz pulse train, of about 110 nJ pulse energy before the compressor, when pumped by frequency doubled, CW DPSS laser (Verdi-10, Coherent) at 532 nm with the output power of 7.7 W. After the external prism compressor and additional acousto-optical modulator the output power can be around 1.1 W, corresponding to the pulse energy of about 100 nJ. The use of broadband, highly chirped mirrors in the laser cavity enables to compensate the dispersion of all intra-cavity components and to achieve the pulse duration of less or about 50 fs (FWHM) [10]. Spectral width of the laser is 35 nm. Wider spectra seem to be problematic due to limitations imposed by saturable Bragg reflector (SBR) mirror in commercial versions. Without the SBR the same system produces 26 fs pulses with more than twice larger output energy [18, 19]. Because of the bandwidth and moderate pulse energy both beam delivery and attenuation optics have to be carefully designed to avoid losses and temporal pulse broadening. We use low dispersion, high-reflection, broadband, dielectric mirrors (Layertec), and a pair of near-Brewster-angle, broadband, thin-film polarisers followed the achromatic half-wave-plate (Altechna), the latter was installed on rotation stage MI423 (Physics Instruments) providing computer control of the power attenuation with more than two millions steps per turn. The state of polarisation of the beam after the attenuator can be changed by additional wave-plates. For inscription experiments we routinely use glass micro-objectives (MO) with numerical apertures of more than 0.55. Additional dispersion induced by the glass in the MO is pre-compensated by tuning the compressor. Overall, our design of optical micro-fabrication system (Fig. 1) enables pulse energies on target of up to 75 nJ, which turns out to be sufficient for processing of all types of glass as well as majority of crystals, including the hardest YAGs. Based on preliminary trials we limited the inscription depth range to 200
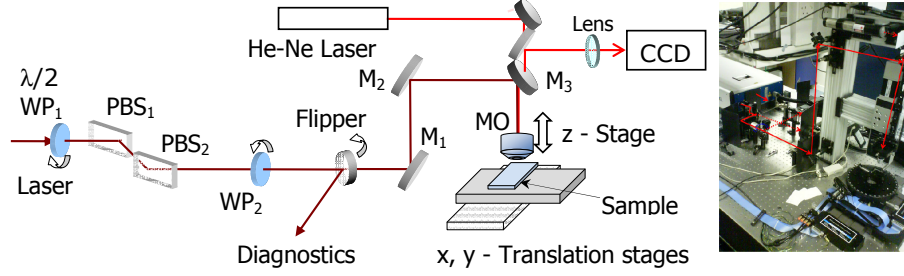
Fig. 1. Experimental setup for inscription with high-repetition rate fs laser and its photo.

μm (this is defined by the type of the micro-objective used). The range of inscription depths can be increased from 12 μm to 800 μm by choosing different focusing conditions.

3.   Experimental results and discussions

3.1.   Refractive index visualisation and reconstruction

The glass sample with written waveguides was first studied by optical microscope (Zeiss, AxioScope-2MOT), equipped with Differential Interference Contrast (DIC) optics, as well as Quantitative Phase Microscopy (QPM) software (by IATIA) with the possibility for RI contrast reconstruction by using Abel inversion and inhouse software, assuming a cylindrical symmetry in the structures obtained. The index reconstruction procedure was calibrated by measuring optical fibres with known specifications at different wavelengths to ensure minimum chromatic aberrations of the system. The reconstructed RI profiles allowed us to simulate waveguide propagation by using finite element method (COMSOL Multiphysics). When compared with experimental observations of the intensity distributions of a several WG modes we observe both good quantitative agreement between experimental and simulation results. This enabled us quantitative comparison of tracks obtained with different inscription regimes and thus ultimate optimisation of inscription parameters [10] in borosilicate glass.

Typical example of a track inscribed by HRR fs laser system is presented on Fig. 2(a). Note the transition form smooth (uniform) WG to a self-arranged quasi-periodical structure for forward translation direction only. These effects can be explained by slight tilting of the phase wavefront, which most likely originate from the micro-objective misalignment but not from the compressor, as for example was stated in the [20]. The reconstructed RI distributions are plotted on Fig. 2(b). Note, that dips in the cross-section of the RI, surrounding the main (positive) RI-peak, are more pronounced at a lower speeds.

3.2.   Results of compositional and structural studies

Structural characterization of the experimental samples with written waveguides was carried out with Raman spectroscopy. Spectra were obtained with Senterra Dispersive Raman Microscope in backscattering geometry at room temperature. Laser beam at 532 nm was focused with $\times 40$ micro-objective to spot of about 2 μm in diameter. The laser power below 10 mW was used to keep off photo-induced phenomena. The measured Raman spectra were normalized with respect to the total bands intensity. The glass sample with written waveguides was stud-
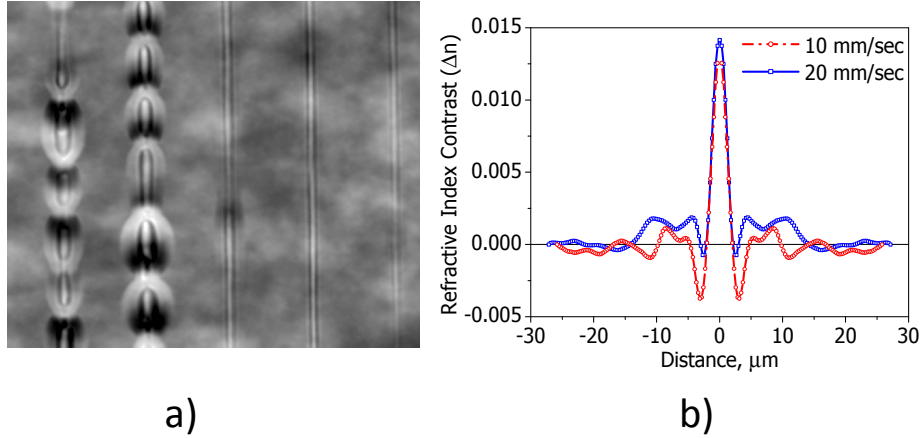
a)   b)

Fig. 2. Microscopic view of the WGs in $0.5Li_2O$-$0.1Nb_2O_5$-$0.4P_2O_5$ glass at 10 (first two tracks from the left) and 20 mm/sec (next two tracks) inscription speed (a). Note the 'wings' on a reconstructed RI profile are more pronounced at a lower speed (b).

ied with scanning electron microscope Zeiss Merlin equipped with the energy dispersive X-ray spectrometer (EDX) Oxford instruments Inca X-act and scanning helium ion microscope Zeiss Orion. Backscattered electrons (BSE) signal was registered with conventional semiconductor detector. SEM and EDX analysis was carried out for the cross-section of written waveguides. The sample was prepared by cutting, grinding and mechanical polishing with Leica EM-TXP system. Alcohol-based lubricants and suspensions were used during polishing procedure to avoid the sample hydrolyzes. The observed BSE image of the waveguides cross-section originates from material contrast (not the surface relief) that is confirmed by comparison with images, obtained by secondary electrons (SE) registration. BSE yield of the glass was calculated as an average yield of all elements with expression suggested in [21]. Monte-Carlo modeling [22] was performed to estimate BSE energy distribution changes for different elements concentration. Negligible BSE energy distribution changes were obtained for investigated samples so BSE detector nonlinearity can be neglected [21]. It should be noted that interaction volume in investigated samples for electrons with energy of 10 keV is about 2 μm , BSE emission volume is about 800 nm, X-ray emission depth is about 1.5 μm and X-ray intensity radial distribution has a radius about 100 nm [22], what provides sufficient spatial resolution for EDX measurements in scan regime.

3.2.1. Raman spectroscopy

The measured Raman spectrum of unmodified sample is shown in Fig. 3(a). The observed bands correlate with specific vibrations associated with Nb-O bonds and structural units of phosphate glass matrix [15-19]. The low-wave number peaks at 600 cm^{-1} and below are assigned to network vibrations [13]. The bands at 600, 760 and 1100–1200 cm^{-1} are attributed to symmetric and asymmetric stretching vibrations of phosphorous tetrahedra units (–P–O–P–, (PO_2) bonds) [13,23,24]. Band at 910 cm^{-1} is connected with vibrational mode of Nb–O bond in $[NbO_4]^{2-}$ units [25, 26].

In this way the Raman spectroscopy allows to conclude that the studied glass has hybrid niobium-phosphate structure based on typical for phosphate glasses flexible –P–O–P– network
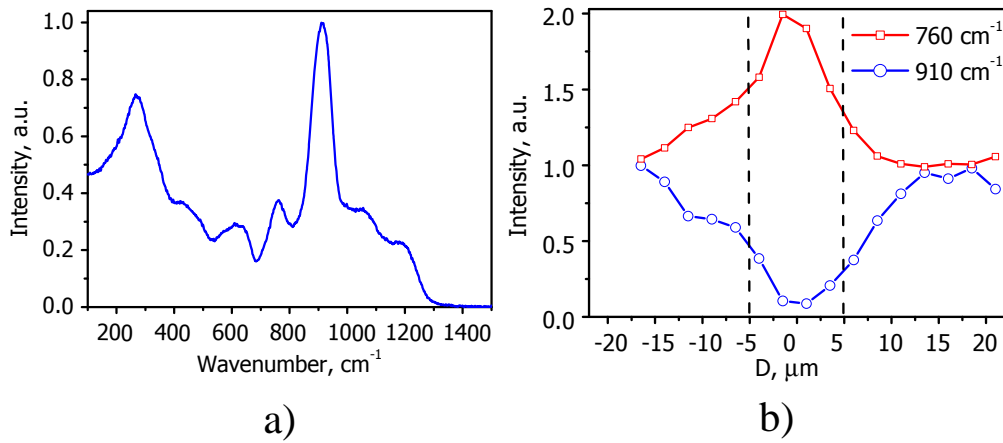
Fig. 3. Measured Raman spectrum (a), of unmodified $0 \cdot 5\,Li_2O - 0 \cdot 1\,Nb_2O_5 - 0 \cdot 4\,P_2O_5$ glass; Intensity of the 760 cm^{-1} (Nb–O) and 910 cm^{-1} (–P–O–P–) bands as a function of position along the cross-section of the waveguide (b).

with embedded Nb-based fragments. At that P ions are five-coordinated and each Nb-ion is six-coordinated by oxygen. Li ions in all probability are built-in phosphate fragments with break of P–O–P bridge bonds and formation of Li^+O^- – P units, and in niobium fragments they may occupy vacancies near (or left by) oxygen of $[NbO_4]^{2-}$ units [27, 28].

Series of Raman spectra measured as a function of position along a waveguide cross-section with step 2.5 μm have not revealed any spectral shift of bands, while the roughly proportional intensity change of peaks located at 760 cm^{-1} (Nb–O bond) and 910 cm^{-1} (–P–O–P– units vibrations) were found. Figure (3(b)) shows intensities of the 760 cm^{-1} and 910 cm^{-1} bands as a function of position along the cross-section of the waveguide. One can see an increase of peak intensity connected with Nb–O bond and intensity decrease of the –P–O–P– units vibrations in the laser modified area. In such a way one can conclude that laser irradiation initiates the Nb–O–P network break with partial switching of bonds P–O–P to Nb–O–P what results in Nb coordination increase from *VI* to *VII*. In accordance to [29] there are two ways of Nb *VII*-coordination realization – pentagonal bi-pyramid and incorporation of oxygen ion to a plain of niobium-oxygen octahedron, resulted in stress formation in laser-affected area.

3.2.2. SEM and EDX analysis

EDX analysis was used to study the distributions of O, P and Nb elements in the sample where no WG were created, at that the measured weight concentrations of 59.6, 15.55 and 3.94 at %(correspondingly 48.5, 24.5, and 18.6 wt %) coincides with synthesis concentrations (or nominal composition) with the error not more than 2.5 at %(or 1 wt %). The observed trace amounts of Al originate from alundum crucible and may be considered as a matrix stabiliser. Concentration of Li was calculated from measured BSE contrast and found to be 18.98 at %(or 6.7 wt %), with synthesis concentration of 20 at %, what demonstrates good measurement accuracy. To study the elements spatial distribution across the fs-WGs the EDX analysis in scan regime was applied. The scanned zones are shown as X and Y lines in Fig. (4(a)). The scanning direction is marked as arrow. Concentration profiles of all elements except Li were measured with EDX analysis, Li concentration was calculated from BSE contrast. The EDX scan measurements demonstrated that concentration of O, P and Al elements do not change along scanned zones within measurement error, however considerable variations of Nb and Li concentrations were observed.

Figures 4(b)–4(c) show concentration change ($\Delta C = C_{\text{scanned zone}} - C_{\text{glass}}$) of spatial distribu-
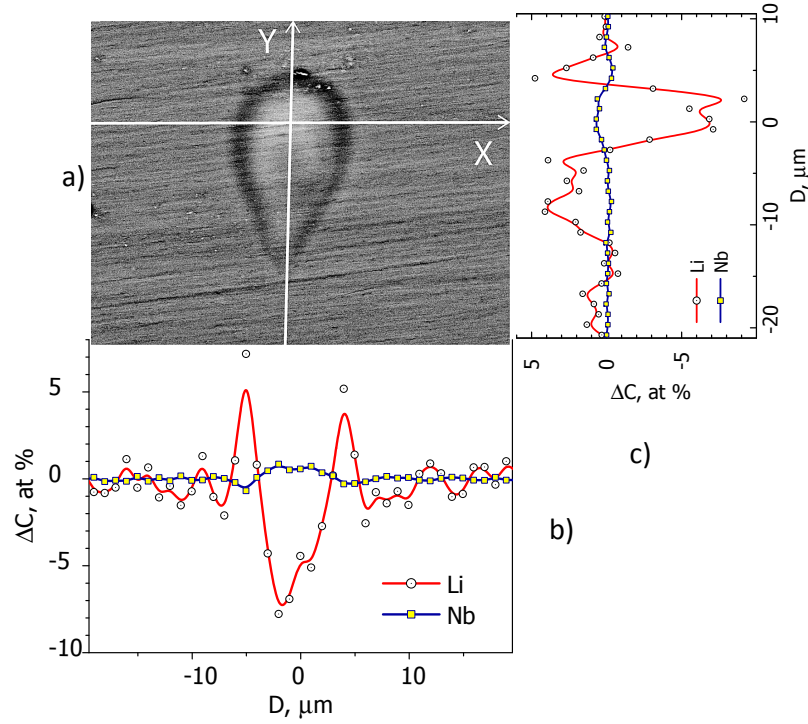
Fig. 4. SEM image (a) and concentration profile of Li and Nb components obtained in scan regime along axis X (b) and axis Y (c). The scanning directions are marked by corresponding arrows.

tion of Nb and Li elements along scanned lines. As it is seen from Fig. 4, change of Nb element concentration is rather moderate about $0.2 \div 0.8$ at% relatively to average concentration in glass, whereas Li demonstrates considerable change of spatial distribution up to $6 \div 8$ at%. The other feature is strong difference of elements spatial spreading: X axis elements distribution is symmetrical relatively to the waveguide center, whereas elements distribution along axis Y has pronounced asymmetry (repeats the drop-shaped cross section of waveguide) in all probability due to specific shape of focal spot, induced thermal lens and so on. Both X and Y distribution of Nb element is characterized by concentration increase in the waveguide center up to $0.6 \div 0.8$ at% and decrease up to $-0.2 \div 0.4$ at% at the distance about 5 μm relatively to average concentration in glass for X direction and 5–7 μm for Y axis. As for Li distribution the concentration drop off up to -8 at% in the central part of waveguide with increase up to $4 \div 6$ at% at the distance 5 μm, followed by reduction to average Li concentration in glass was observed. In such a way EDX analysis demonstrated that the written waveguide is characterized by special chemical composition (Li deficit – -8 at% and Nb excess 0.8 at%) in comparison with the initial glass. The observed local variation of glass composition can be explained in terms of elements migration (apart a smaller increase in Li concentration below the focal region - in the direction of light propagation). Note that such a peculiarities in materials modification along the laser beam have been observed by a number of research groups [8, 10, 19]. Fs laser irradiation in HRR regime induces strong local heating of the material, up to $1000 \div 2000°C$ [10, 11, 19]. As the studied phosphate glass has T_g about 520°C, the laser affected zone can be considered as melt where chemical compounds are thermally dissociated to ions and/or ions associates. High temperature gradient induces thermal diffusion of first of all Li^+ ions as the most mobile and light element. As a result Li^+ depleted region gains negative space-charge field due to oxygen

excess above stoichiometry. At the used laser parameters and sample translation velocity the cooling rate of the laser-affected zone is extremely high $10^5 \div 10^6 \, K/\mathbf{s}$ what bounds oncoming Li migration caused by concentration diffusion and space-charge field. In such a way, the final spatial distribution of Li element is determined by variety
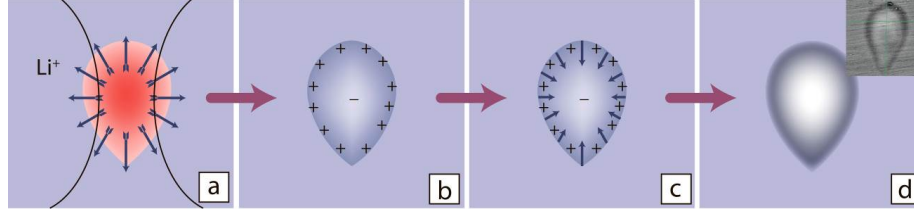

Fig. 5. Scheme of the laser-induced processes developing in the studied glass: thermal diffusion (a), space-charge field (b), concentration diffusion and migration in internal electric field (c), resulted SEM material contrast (d).

of processes which are schematically illustrated in Fig. 5: thermal diffusion (a), resulted in formation of a space-charge field (b), followed by concentration diffusion and migration in internal electric field in reverse direction (c). It should be noting that the oncoming migration processes (c) have not such a strong effect on Li distribution in comparison with thermal diffusion (a) due to extremely fast material resolidification.

The observed local increase of Nb^+ ions concentration is most probably connected with matter/ions redistribution in the waveguide center due to attraction of positively charged Nb-containing fragments (for example $[NbO_{4/2}]^+$) to negatively charged, Li^+ depleted area. Similar effect of charge compensation was found for Li-deficient $LiNbO_3$ crystals, were in accordance to model of Abrahams and Marsh [30] each missing Li^+ ion is replaced by an Nb^{5+} ion with compensating vacancies at the Nb site maintaining charge neutrality. The resulted mechanical stresses lead to formation of thickened area surrounded by less dense material what appears as Nb concentration decrease at distance of about 5 μm . The variation of the chemical composition of the matrix determines optical properties change – refractive index in particular. For example, for $LiNbO_3$ crystals the decrease of Li concentration on $2 \div 3$ at% results in a strong refractive index increase up to $0.03 \div 0.05$ [17]. In our case the observed considerable laser-induced modification of local glass composition also results in strong refractive index (RI) change, at that spatial RI variation is well correlated with Li and Nb distributions as illustrated in Fig. 4.

Also, we have made a few attempts to synthesis LNP glasses with variable concentrations of Li/Nb in order to compare bulk refractive indices of such glasses with measured induced RI values, however in most cases we observed citallisation. This means that such concentration deviations of elements cannot be formed by classic process of glass synthesis in 'equilibrium' conditions. In Li_2O-P_2O_5 glasses (without Nb) our study revealed that the decrease in Li concentration from 18.36 to 17.3 at %produces increase of the bulk refractive index from about 1.50 to 1.53.

Finally, in recent experiments by Turchin et. al. [4, 5] in a multicomponent (borosilicate) glass the appearance of anisotropic light scattering was observed, emerging from the center of fs-irradiated (melted) area after the fs laser was switched off. We believe that much faster cooling rate obtained in experiments mentioned above was, most likely, accompanied by the pressure wave generated during the collapse of melted bubble, leading to the creation of some nano-crystals inside irradiated volume. Apparently, much softer heating and cooling protocols,

occurring in our experiments on WG fabrication in LNP glasses,were not efficient for growing of nano-crystals.

4. Conclusion

In conclusion, we demonstrate high-contrast WGs fabricated by direct femtosecond laser inscription at high-repetition rate in lithium niobo phosphate glasses, and demonstrated that fs laser irradiation provides unique tool for accessing and transforming materials beyond static equilibrium states. Our work proves that fs modification at final stage involves non-local material transformations, atom/ions redistributions or chemical changes in material, which may be the dominant mechanism for the RI contrasts induced in multicomponent glasses. Despite non-equilibrium phase-states of materials achieved, the range of quite moderate sample translation speeds used did not facilitate creation of nano-crystals in the bulk of LNP glass. Slower processing protocols may be an advantage if main focus is on changing local material composition.